Available online at www.sciencedirect.com
SCIENCE DIRECT
Agricultural and Forest Meteorology 133 (2005) 40–53
AGRICULTURAL AND FOREST METEOROLOGY
www.elsevier.com/locate/agrformet

Atmospheric response and feedback to radiative forcing from biomass burning in tropical South America

Yongqiang Liu *

Forestry Sciences Laboratory, USDA Forest Service, 320 Green Street, Athens, GA 30602, USA

Received 26 January 2004; received in revised form 26 January 2005; accepted 7 March 2005

Abstract

Simulations are performed to understand the importance of smoke from biomass burning in tropical South America to regional radiation and climate. The National Center for Atmospheric Research (NCAR) regional climate model coupled with the NCAR column radiative model is used to estimate smoke direct radiative forcing and consequent atmospheric perturbations during a smoke season in this region. The smoke optical properties are specified based on the measurements during the smoke, clouds, and radiation-Brazil experiment. The simulations obtain a direct radiative forcing of $-16.5\ \mathrm{W\ m^{-2}}$ over the smoke region. This magnitude, however, is substantially reduced due to atmospheric feedback. Clouds and precipitation are reduced due to smoke. The cloud reduction mainly results from smaller water vapor transport from the ground and the planetary boundary layer to the cloud layer because of the combined effects of reduced turbulent activity and the subsidence tendency. The simulated cloud reduction agrees with a recent finding from satellite measurements. Smoke also leads to the enhancement of a dominant planetary-scale high system. A two-layer structure of warmer air with ascending tendency on top of cooler air with descending tendency is formed due to smoke with strong absorption.

Keywords: Biomass burning; Radiative forcing; Regional climate change; Climate modeling

1. Introduction

As one of the sources of atmospheric aerosols (Andreae and Merlet, 2001), smoke particles from biomass burning can affect regional and global radiation through scattering and absorbing solar radiation, a mechanism known as ''direct radiative forcing'' (DRF) (Charlson et al., 1992). DRF is measured by the perturbation in the net solar radiation flux at the top of the atmosphere (TOA) induced by aerosols. Penner et al. (1992) first emphasized the importance of smoke particles to global radiative budget (that is, net fluxes of solar radiation absorbed by and thermal radiation emitted from the earth–atmosphere system). Based on carbon emissions from biomass burning (Crutzen and Andreae, 1990; Hao et al., 1990), that study obtained a globally averaged smoke DRF of about $-1\ \mathrm{W\ m^{-2}}$, which is comparable to that of anthropogenic sulfate aerosols. The negative sign means that the net solar radiation received by the atmosphere–earth system is reduced due to smoke. Large radiative forcing of smoke was also found in Africa during the Southern African Regional Science Initiative (SAFARI 2000) (Swap et al., 2003; Hansell et al., 2003) and in Southeast Asia during the 1997 forest fires (Davison et al., 2004; Kobayashi et al., 2004).

Radiative forcing of atmospheric aerosols can further modify clouds (Hansen et al., 1997). It was observed during the Indian Ocean Experiment (INDOEX) that there was relatively small cloud

* Tel.: +1 706 559 4240; fax: +1 706 559 4245.
E-mail address: yliu@fs.fed.us.

0168-1923/$ – see front matter © 2005 Elsevier B.V. All rights reserved.
doi:10.1016/j.agrformet.2005.03.011

coverage over the ocean area due to the large concentration of soot aerosols, which absorb solar radiation, increase air temperature, reduce relative humidity and, therefore, ''burn out'' clouds (Ackerman et al., 2000). A secondary anti-cyclonic circulation and cloud reduction were found over the eastern U.S. and the adjacent Atlantic Ocean during summer due to aerosols (Liu et al., 2000). Absorbing aerosols were found to be a contributor to the long-term precipitation anomalies in China (Menon et al., 2002).

Two recent measurement studies obtained observational evidence for cloud changes directly related to biomass burning in the Amazon region. Koren et al. (2004) analyzed the satellite measurements from moderate resolution imaging spectroradiometer (MODIS) during the biomass-burning season. It was found that clouds were reduced from 38% in clean conditions to 0% for heavy smoke in the Amazon region. Andreae et al. (2004) analyzed the role of smoke particle in cloud microphysics from field measurements during the large-scale biosphere–atmosphere experiment in Amazonia-smoke, aerosols, clouds, rainfall, and climate (LBA-SMOCC) campaign. It was found that heavy smoke from forest fires reduced cloud droplet size and therefore delayed the onset of precipitation from 1.5 km above cloud base in pristine clouds to more than 5 km in polluted clouds and more than 7 km in pyro-clouds.

One of the major distinct properties of smoke as well as other tropospheric aerosols from greenhouse gases is its large spatial variability due to local origination and relatively short lifetime. Measurements have shown dramatically large amounts of wildland fire emissions in the Amazon and North America (e.g., Ward et al., 1991; Radke et al., 1991; Liu, 2004), making smoke an important factor to radiation budget in these regions. Biomass burning in the tropics, including tropical South America, is of particular interest because of the large extent of forest clearing and agricultural burning. A majority (more than 70%) of the global burned biomass is in the tropics (Seiler and Crutzen, 1980). In addition, the large solar incident flux in the tropics enhances the climatic effects of aerosols (Holben et al., 2001). A number of field experiments have been conducted in the Amazon region, including the biomass burning airborne and spaceborne experiment-Amazonia (BASE-A) (Holben et al., 2001) and the smoke, clouds and radiation-Brazil (SCAR-B) (Kaufman et al., 1998), to measure physical and optical properties of smoke aerosols and estimate their radiative forcing. Large radiative forcing of smoke has been found from measurement (Hobbs et al., 1997) and model calculation (Ross et al., 1998) in the Amazon region.

Various modeling techniques have been used to simulate direct radiative forcing of smoke and climatic effects in the tropics. Atmospheric radiation transfer models (e.g., Ross et al., 1998) are a major tool for estimating radiative forcing. Radiative-dynamical models (e.g. Liu, 2003) and radiative-dynamical–statistical models (e.g. Moraes et al., 2004) are useful to understanding physical mechanisms for the climatic effects of smoke. Regional climate models coupled with state-of-the-art atmospheric radiative transfer schemes provide a powerful modeling tool for understanding the effects of smoke on radiation and interactions with regional climate.

The present study seeks to understand the importance of smoke to regional climate by simulating a smoke season in tropical South America with a regional climate model. A major issue is cloud change due to smoke and the associated mechanisms. The results will provide modeling evidence for the observed cloud reduction over the smoke areas in the Amazon region (Koren et al., 2004). The optical properties of the smoke are specified based on the measurements from SCAR-B. The methods and simulated atmospheric fields are first described in Sections 2 and 3. The results are then presented in Section 4.

2. Methodology

2.1. The model

The National Center for Atmospheric Research (NCAR) regional climate model (RegCM) (Dickinson et al., 1989; Giorgi and Bates, 1989) is used to simulate atmospheric response to smoke aerosol radiative forcing. RegCM characterizes regional features of climate and land-surface processes at geographic regions of interest by incorporating the NCAR Column Radiative Model (CRM, Kiehl and Briegleb, 1993), the Grell convective parameterization (a scheme to estimate rainfall within a grid cell) (Grell, 1993), and the biosphere–atmosphere transfer scheme (BATS, a scheme to estimate momentum, heat, water, and other mass exchanges on the air–land interface and predict variations in soil and vegetation temperature and moisture) (Dickinson et al., 1993) into the standard NCAR/Penn State Mesoscale Model (MM4/5) (Anthes et al., 1987; Grell et al., 1994). RegCM was found to be able to reproduce important high-resolution spatial characteristics of climate for major geographic regions over the world (e.g., Dickinson et al., 1989; Giorgi and Bates, 1989; Liu et al., 1996). The latest version of RegCM (Giorgi et al., 1999) is used in this study.

CRM has 18 discrete spectral intervals for the solar spectrum. Calculation of the radiative effects of atmospheric aerosols is included. It has been coupled with global and regional climate models to simulate regional transport, and radiative and climatic effects of aerosols (Qian and Giorgi, 1999; Kiehl et al., 2000; Giorgi et al., 2002).

2.2. Simulation set up

The atmospheric response, including perturbations in cloud, temperature, humidity, and geopotential height, is simulated for August and September of 1995 with RegCM. Fig. 1 shows the simulation domain. The Andes Mountains stand in the Pacific coast with the highest elevation of 4.5 km. Smoke is assumed to cover the shaded area. The domain has a resolution of 60 km with 91 × 91 grid points and 14 vertical layers up to 80 hPa. The time step is 1 min.

The initial and horizontal lateral boundary conditions of wind, temperature, water vapor, and surface pressure are interpolated from the analysis of the European Center for Medium Range Weather Forecast (ECMWF), whose resolution is 1.875° of latitude and longitude. Soil water content is initialized depending on type of vegetation (Giorgi and Bates, 1989). Sea-surface temperature (SST) is interpolated from a set of observed, monthly mean with a resolution of 0.5° (Shea et al., 1992). A set of station data of observed monthly precipitation and the surface air temperature from the U.S. National Center for Environmental

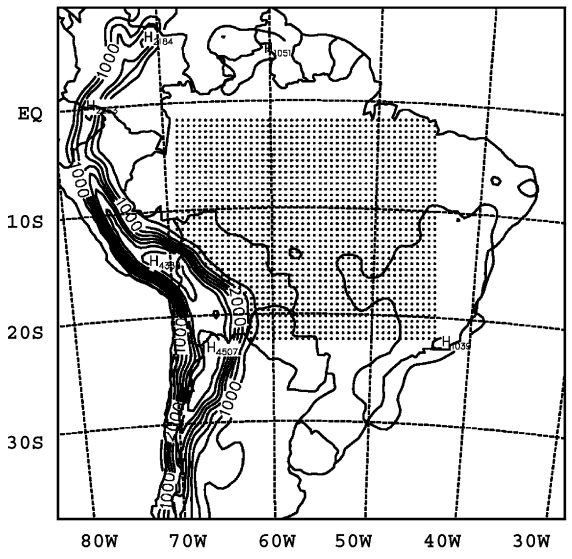

Fig. 1. The simulation domain with the smoke region shaded by dots. The interval of topography is 500 m.

Table 1
RegCM simulations

Simulation	TOD	SSA	Smoke layer height
Control	0.0	0.0	N/A
Smoke	0.75	0.88	∼2.5 km
Smoke-strong absorption	0.75	0.82	∼2.5 km
Smoke-weak absorption	0.75	0.94	∼2.5 km

TOD and SSA stand for total optical depth and single scattering albedo.

Prediction (NCEP) is used to evaluate model performance. All these data were obtained from archives of the NCAR Scientific Computing Division.

A control simulation without smoke loading and a smoke simulation with smoke loading are conducted (Table 1). DRF of smoke is approximately measured by the difference in the net solar radiation flux at the top model level between the smoke and control simulations. Atmospheric response is measured by the differences in various atmospheric fields (cloud, temperature, humidity, circulation, surface energy and water balance components, etc.) between the two simulations.

In the smoke simulation, the smoke optical properties, including total optical depth (TOD, an optical index measuring smoke loading), single scattering albedo (SSA, an optical index of the ratio of scattering to the sum of scattering and absorption of smoke) and asymmetric factor, are specified based on the SCAR-B measurements. The midvisible optical depth of 0.75 is adopted (Ross et al., 1998) for the smoke region. The land areas other than the smoke region and the Andes Mountains are assumed to have a background optical depth of 0.12. An SSA of 0.88 is specified for the smoke approximately at 0.55 μm based on the measured range of 0.82 for young smoke and 0.94 for aged smoke (Eck et al., 1998). Two more simulations (smoke-strong absorption and smoke-weak absorption in Table 1) with the SSA values of 0.82 and 0.94 are conducted to understand the role of the smoke absorption property. Wavelength dependencies of the optical properties are determined mainly based on the fourth-order polynomials (Ross et al., 1998). Humidification effect has been included in the optical depth.

Actual horizontal pattern and vertical profile are very complex for a number of reasons. First of all, burning takes place at individual locations with different fuel properties and meteorological conditions. Secondly, burning activities and meteorological conditions vary over time. Thirdly, smoke particles can be transported from burning areas. It was found during a period of the SCAR-B experiment that smoke particles below 2 km were transported westwards by the prevailing airflows,

which led to a large concentration of smoke particles on the eastern side of the Andes Mountains. Some particles were further moved southwards until 20°S (Trosnikov and Nobre, 1998). For biomass burning over southern Africa where there is no barrier of high mountains along the coasts, it was found that a substantial amount of smoke particles was transported to the adjacent Atlantic and Indian Oceans (Sinha et al., 2004). Lastly, spatial and temporal variability of smoke will be affected by smoke–atmosphere interactions.

A simplified case of smoke distribution is adopted for this study. Smoke particles are assumed to be retained within the smoke region and to be evenly distributed in a layer between the ground and about 2.5 km throughout the simulation period. The height of 2.5 km is specified based on the measured profiles of smoke particles (Ross et al., 1998). The averages of smoke optical properties over the smoke season are used, which remain the same during the entire integration period.

Smoke particles can also act as cloud condensation nuclei (CCN) and change cloud droplet size distribution, which leads to cloud change (Andreae et al., 2004) and indirect radiative forcing (e.g., Twomey et al., 1984; Kaufman and Tanre, 1994). These changes may have a comparable or even greater role in modifying regional circulation and cloud patterns than that due to direct radiative forcing. This role, however, is not examined in this study.

2.3. Feedback

The total radiative forcing of smoke simulated with RegCM is the perturbation in net solar radiation flux at the top model level due to two processes. One is scattering and absorption by smoke, which is the traditionally defined direct radiative forcing. The second one is the change in cloud reflection and absorption of solar radiation, which is caused by cloud modification resulting from the first process. The perturbation due to the second process will be regarded as feedback of atmospheric response to smoke radiative forcing in this study.

To roughly estimate the effect of the feedback on radiative forcing, CRM is run off-line at individual RegCM grids within the domain shown in Fig. 1 at four times (i.e., 0, 6, 12, and 18 GMT). Air temperature and humidity, cloud fraction and water path at each grid are specified using the RegCM simulation outputs averaged over the simulation period from 1 August to 30 September 1995.

Three CRM simulations are conducted (Table 2): (a) control simulation without smoke and using meteorological fields from the RegCM control simulation, (b) smoke simulation, which is the same as (a) except with smoke, and (c) smoke-feedback simulation, which is the same as (b) except with the cloud fraction and cloud water path from the RegCM smoke simulation. The difference in the net solar radiation flux at the top of the model level between the simulations (b) and (a) approximately measures DRF of smoke particles without cloud feedback, while that between the simulations (c) and (a) measures DRF with cloud feedback.

Note that RegCM simulated radiation processes and atmospheric fields (temperature, humidity, cloud, etc.), both of which are modified by smoke, interact with and feedback to each other at each time step of the integration. In the CRM simulation, however, cloud change, obtained from the RegCM simulations, acts as a driving factor for radiation processes. The change in the radiation processes due to the cloud change does not feed back to cloud and other atmospheric fields. Also, the feedback of clouds might be more significant under certain atmospheric conditions during a specific short period, but the CRM simulation would be unable to catch such short-term signals because the average of clouds over the 2-month integration period simulated with RegCM is used.

3. Simulated atmospheric fields

Three RegCM simulated fields are analyzed and compared with the ECMWF analysis and the NCEP observation to briefly illustrate the atmospheric background during the smoke season of 1995 over South

Table 2
CRM simulations

Simulation	Aerosol optical properties	Meteorological fields
Control	Same as RegCM control simulation	From RegCM control simulation
Smoke	Same as RegCM smoke simulation	From RegCM control simulation
Smoke-feedback	Same as RegCM smoke simulation	From RegCM control simulation (T, H) and smoke simulation (cloud)[a]

[a] T and H represent temperature and humidity.

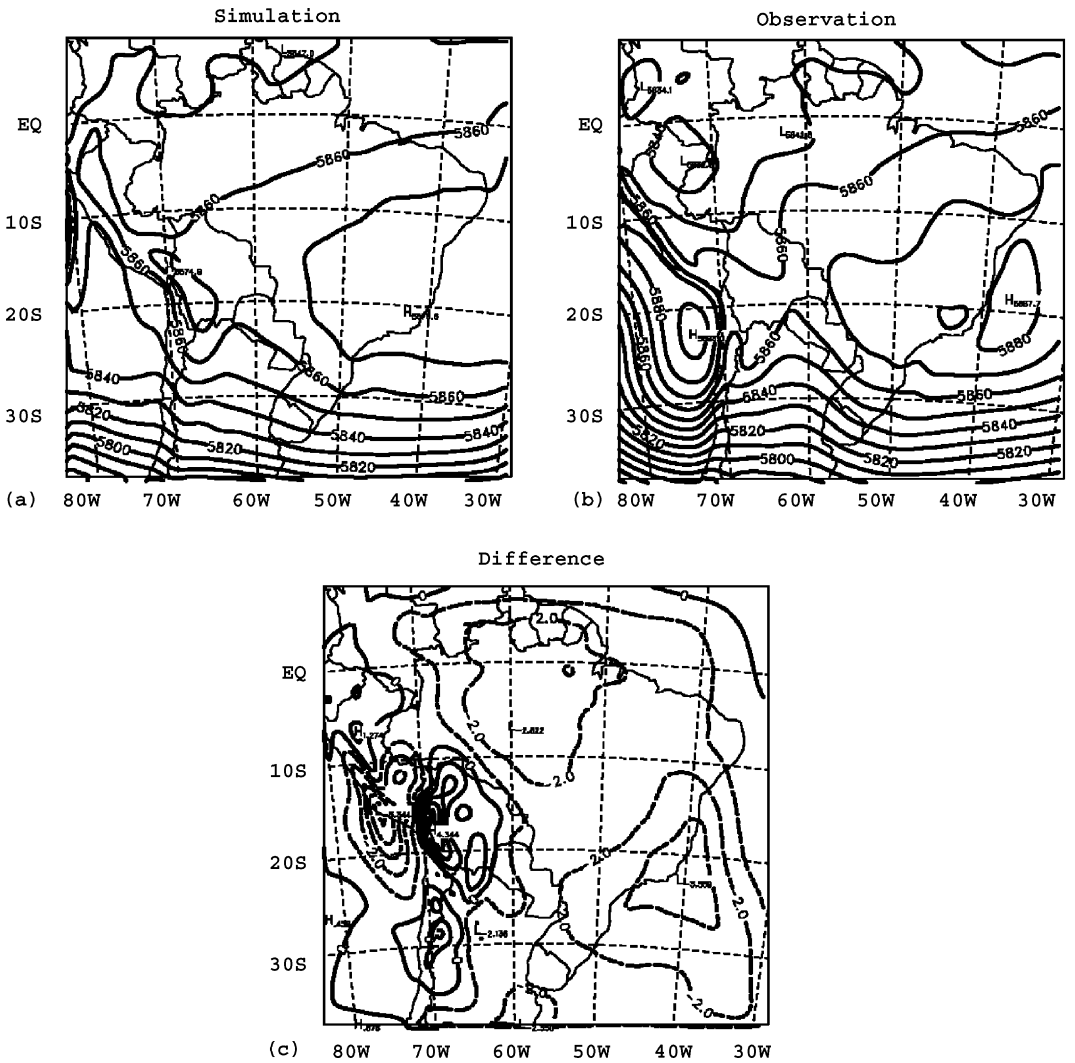

Fig. 2. Geographical patterns of 500 hPa geopotential height (m) for August–September 1995. Panels (a)–(c) are the RegCM simulation, the ECMWF analysis, and the difference between (a) and (b). The contour intervals are 10 m for (a) and (b) and 1 m for (c). Solid and dashed lines represent positive and negative values, respectively.

America and to evaluate model performance. In the simulated 500 hPa geopotential height (Fig. 2(a)), a planetary-scale high is dominant over Brazil. In the mid-latitudes is the westerly jet region with a weak trough, whose north–south oriented trough line is located east of the Andes Mountains between 62° and 64°W. There is a high center along the Pacific Ocean coast at about 20°S. Over the Caribbean Sea coast is a tropical trough. The simulated rain regime extends from the Caribbean Sea coast to the Andes Mountains and to the Atlantic Ocean off the southeastern Brazil coast (Fig. 3). There are a number of areas with monthly rainfall over 100 mm. Monthly rainfall over most of the smoke region, however, is less than 40 mm. The simulated surface air temperature (Fig. 4) shows a warm area of about 30 °C over the smoke region and the adjacent areas. Temperature gradually decreases towards south. Low temperature is found over the Andes Mountains as well as the coastal Brazil Plateau because of the high elevations.

This simulated spatial pattern of the above three fields shows some important similarities to, but also some important differences with the ECMWF analysis or the NCEP observations. The model underestimates the intensity of the high system over the Pacific Ocean and the tropical trough in comparison with the ECMWF analysis. Note that the ECMWF analysis is a combination of sounding observation and modeling with a

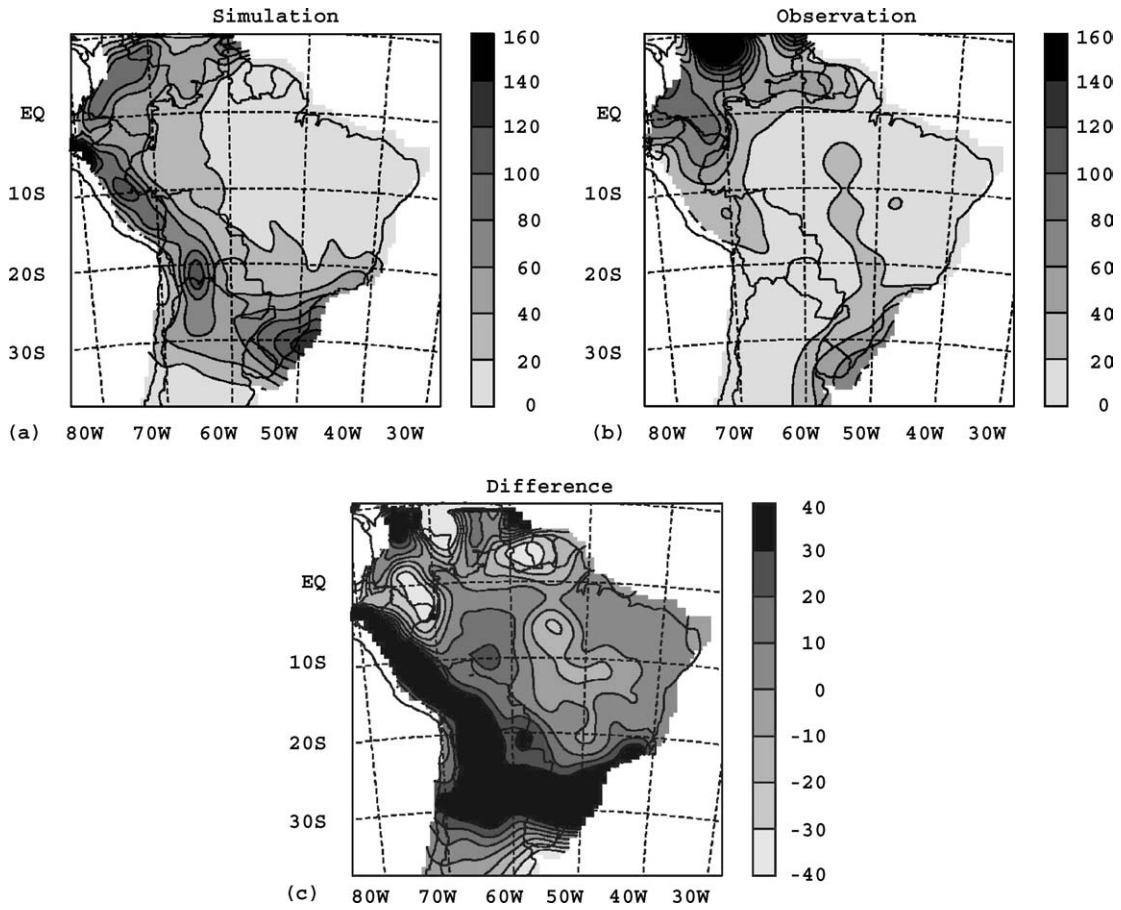

Fig. 3. Geographical patterns of the monthly rainfall (mm) for August–September 1995. Panels (a)–(c) are the RegCM simulation, the ECMWF analysis, and the difference between (a) and (b).

global model. The analysis over the areas without sounding observation (e.g., oceans and mountains) is actually model output. The simulated rainfall is generally larger than the NCEP observations in the southern Andes Mountains. This could indicate an overestimate of rainfall by RegCM, or missing observations in the NCEP data in this region. This simulated air temperature is about 2 °C higher in the southwest portion of the smoke region. Experiments indicate that the surface temperature is sensitive to initial soil moisture. Because of unavailability of this important soil property in most cases, initial soil moisture is specified based on land cover type in RegCM, which is expected to be one of the sources for uncertainties in the surface temperature simulation. Another factor is the effect of smoke. It will be described in the next section that the surface air temperature averaged over the smoke region is reduced by 1 °C due to smoke. This suggests that the magnitude of the overestimate of the surface air temperature would be significantly smaller if smoke is included in the simulation.

A reliable simulation of atmospheric processes is essential to understanding the effects of smoke on regional climate. As in other climate models, cloud and precipitation calculation has great uncertainty (e.g., Liu et al., 1996). The continuous efforts in developing parameterization schemes of these processes and their interactions with atmospheric particles and radiation are critical to improving simulation of smoke's effects on regional radiation and climate.

4. Results

4.1. Direct radiative forcing of smoke

Fig. 5 shows DRF without feedback simulated with CRM. The DRF is about -15 W m^{-2} or stronger in magnitude over the smoke region. The average over the entire smoke region is -16.5 W m^{-2} (Fig. 6).

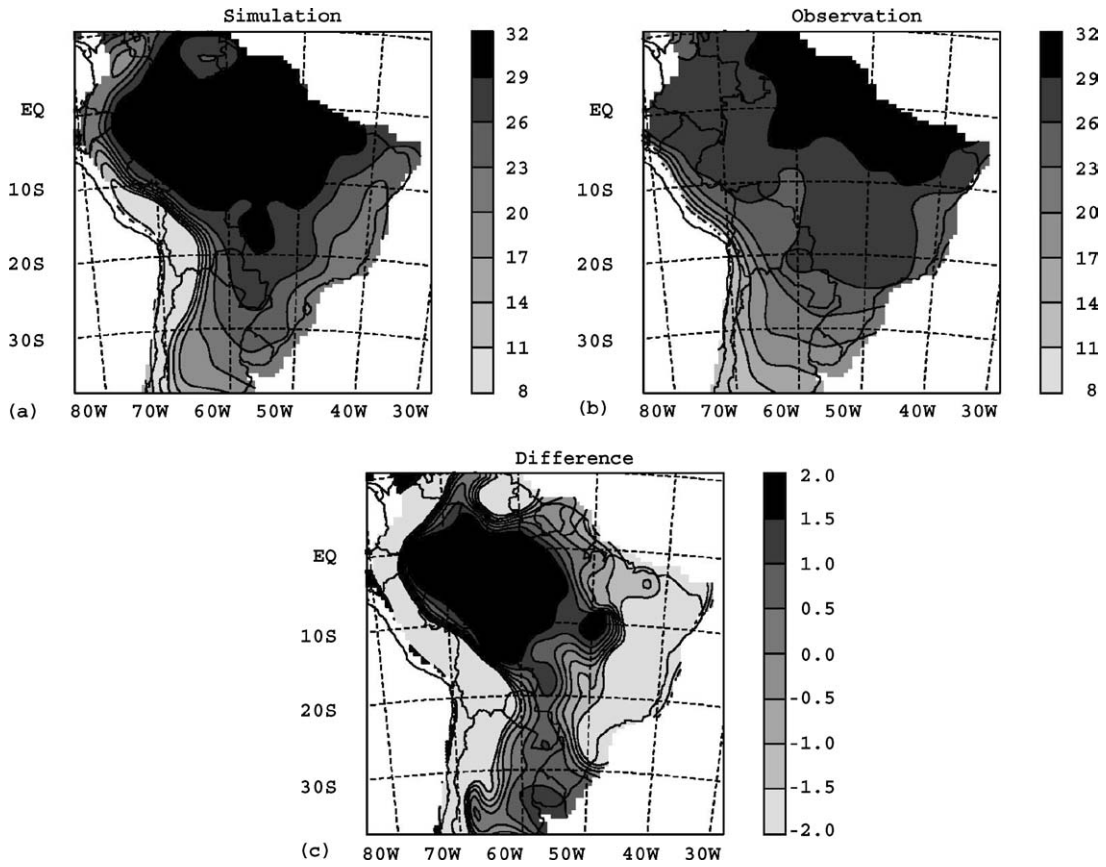

Fig. 4. Same as Fig. 3 except for the surface air temperature (°C).

4.2. Effect on clouds

Fig. 7 shows spatial distribution of the difference in cloud water path accumulated from 1 to 4.5 km in the vertical direction between the RegCM control and smoke simulations. Large reduction occurs in the smoke region. Fig. 8(a) shows vertical profile of cloud water path between the two levels of each layer. Reduction in cloud water path occurs mainly between 2 and 4 km with the magnitude of 10 g m^{-2}, which is about 40% of the original amount.

Besides the smoke region, cloud reduction due to smoke is also found northwest and southeast of the region. This teleconnection effect is caused by the enhancement of the planetary-scale high system over the South America, as shown below. Smoke can also affect areas outside the smoke region through advection of smoke. This teleconnection effect is not examined in this study. According to modeling with a smoke transport model (Trosnikov and Nobre, 1998), smoke particles emitted from biomass burning in the Amazon below 2 km during a period of the SCAR-B experiment were first transported westwards to the eastern side of the Andes Mountains and then moved southwards. It is expected that the teleconnection effect due to smoke advection would mainly appear on the eastern side along the mountains during the SCAR-B experiment period.

4.3. Processes responsible for the cloud reduction

4.3.1. Thermodynamics

Smoke can directly affect atmospheric thermodynamics through absorbing solar radiation. The original heating rate of radiation (Fig. 8(b)) is positive, indicating that the gain from the absorption of solar short-wave radiation by water vapor, cloud droplets, and other trace gases is greater than the loss from long-wave radiation to space. The maximum heating rate is about 1.2 °C per day at the cloud layer around 3 km. Smoke causes an increase in the heating rate perturbation below 2 km with the largest perturbation of about 2.4 °C, which is twice as large as the original maximum heating rate.

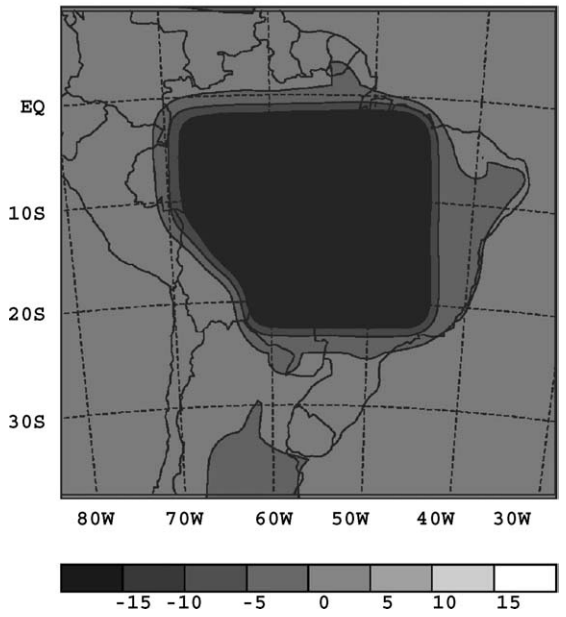

Fig. 5. Direct radiative forcing of smoke (W m^{-2}) without atmospheric feedback simulated with DRM (that is, the difference in the net solar radiation flux at the top model level between the smoke and control simulations).

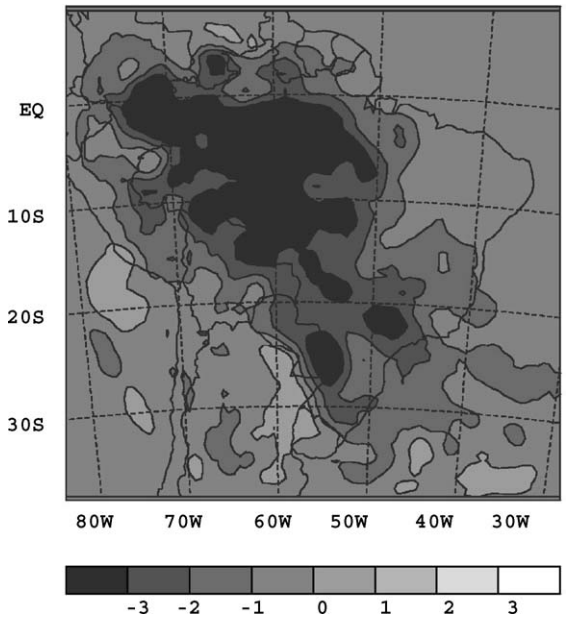

Fig. 7. Perturbation in cloud water path (g m^{-2}) due to smoke, averaged over the levels between about 1 and 4.5 km.

Despite a slight increase in air temperature in the cloud layer corresponding to the positive perturbation in the heating rate, air temperature is overall reduced below 2.5 km with a magnitude of about -1 °C on the ground (Fig. 8(c)). The cooling is found to result from the perturbation in the surface energy balance. The original net solar radiation (Fig. 9) on the surface is about 240 W m^{-2}, consumed by long-wave radiation (95 W m^{-2}), sensible heat flux (75 W m^{-2}), and latent heat flux (70 W m^{-2}). Solar radiation is reduced by 50 W m^{-2}, about 20% of the original value, due to smoke, which in turn causes a dramatic reduction in sensible heat flux and, therefore, a cooling tendency above. It appears that the role of sensible heat flux is more important than that of smoke absorption of solar radiation in determining air temperature up to the cloud layer.

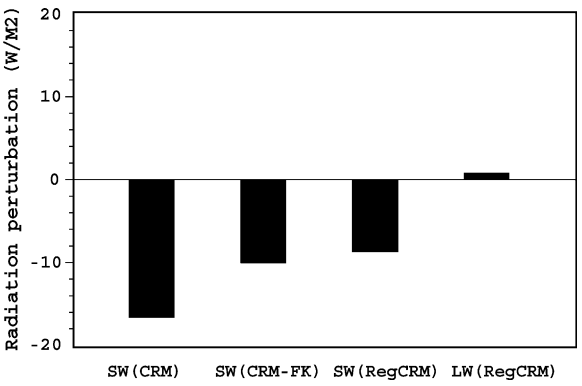

Fig. 6. Average perturbations in net radiation fluxes at the top model level due to smoke over the smoke region. SW (CRM): shortwave flux difference between the CRM control and smoke simulations; SW (CRM-FK): same as SW (CRM) except for the difference between smoke-feedback and control simulations; SW (RegCM): shortwave flux difference between the RegCM control and smoke simulations; and LW (RegCM): same as SW (RegCM) except for longwave radiation flux.

Fig. 8(d) shows pseudo wet-bulb potential temperature, which is proportional to air temperature and water vapor mixing ratio, and inversely proportional to air pressure. Vertical lapse rate of this variable is usually used to measure atmospheric wet static stability. The perturbation in this variable is negative with an increased magnitude until 3 km, indicating a reduced stability that favors cloud development. Note that the vertical profile of the wet-bulb potential temperature perturbation does not follow that of air temperature; instead, it is close to that of water vapor mixing ratio (Fig. 8(e)), which will be described below.

4.3.2. Water transport

The surface water balance is also changed due to smoke. Evapotranspiration is a major component in the original water balance. The average over the smoke region is greater than 70 mm per month, about five

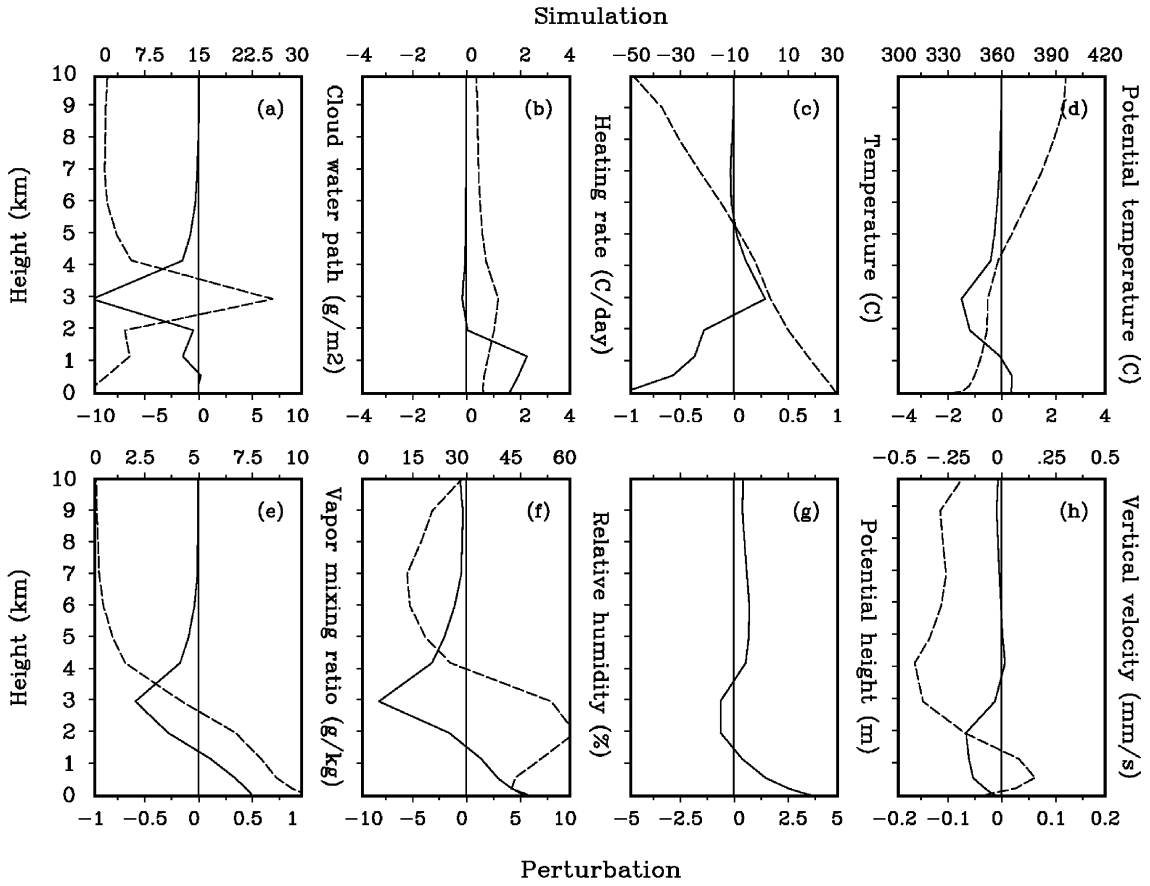

Fig. 8. Vertical profiles of atmospheric variables (panels (a)–(h)) averaged over the smoke region. The dashed lines in all panels except (g) represent the RegCM control simulation with the value labeled at the top of each panel, and the solid ones represent the differences between the smoke and control simulations with the value labeled at the bottom.

times as large as rainfall. Runoff is negligible. Evapotranspiration and rainfall are reduced by 6 and 4 mm per month due to smoke, respectively. The reduction in evapotranspiration means reduced water transfer from the ground to the planetary boundary layer (PBL). The reduced sensible heat flux (therefore, weaker turbulent activity) means weaker water vapor transfer from PBL to the cloud layer. In other words, more water vapor stays in PBL instead of being transported to the cloud layer. As a result, smoke leads to a large negative perturbation in water vapor mixing ratio at the cloud layer.

Relative humidity is a major factor for non-convective rainfall, which is a dominant form of precipitation over the smoke region during dry seasons. The original relative humidity averaged over the smoke region is about 40% on the ground and 60% at the cloud layer (Fig. 8(f)). The perturbation due to smoke is positive in the lowest 2 km with the largest magnitude of 5%, and negative above this layer with the magnitude of nearly 10% at about 3 km, which directly contributes to the cloud reduction.

Relative humidity perturbation is determined by perturbations in water vapor mixing ratio and air temperature, whose relative importance can be roughly estimated using the widely used Magnus empirical formula for saturation water pressure (Murray, 1967). The original temperature (Fig. 8(c)) and water vapor mixing ratio (Fig. 8(e)) are about 1 °C and 5 g kg^{-1} at the cloud layer of 3 km (about 700 hPa), and the corresponding perturbations are 0.25 °C and −5 g kg^{-1}. Relative humidity will be reduced by about −1.5 and −12% in response to the perturbations, respectively. This suggests that the reduction in water vapor mixing ratio should be a major contributor to the reduction in relative humidity.

4.3.3. Circulation

Smoke has a remarkable effect on regional circulation. The perturbation in the 500 hPa geopotential

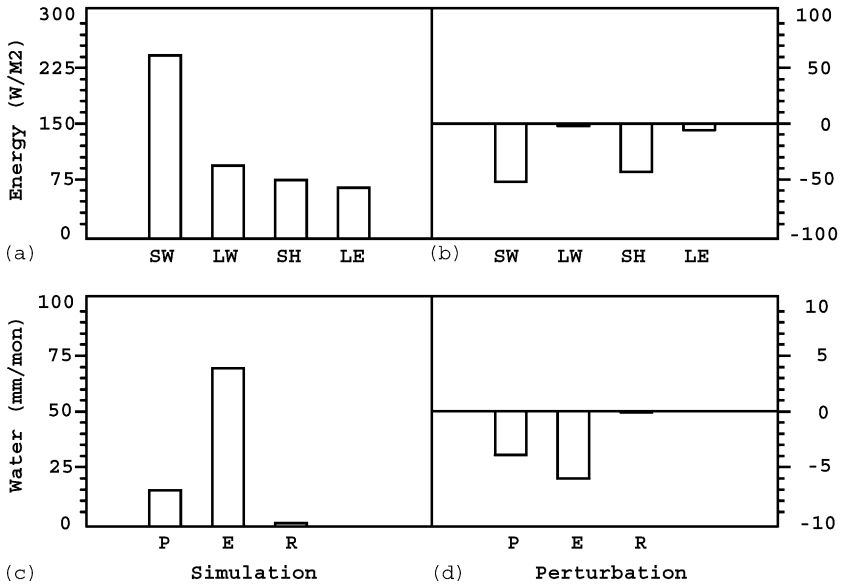

Fig. 9. The surface energy and water balance averaged over the smoke region. Panels (a) and (b) are simulated and perturbed energy balance, and (c) and (d) are simulated and perturbed water balance. The label is on left side for simulation and right for perturbation. SW, LW, SH, and LE represent short-wave, long-wave, sensible heat, and latent heat flux, and P, E, and R represent precipitation, evaporation, and runoff.

height is mostly positive over the smoke region (Fig. 10) with the largest magnitude found over the northwestern portion. This result indicates a tendency of enhanced Atlantic Ocean high or weakened tropical trough.

The sign of perturbation in geopotential height, however, varies with height (Fig. 8(g)). Positive perturbation occurs between about 600 and 275 hPa, and between the ground and about 850 hPa, with a larger magnitude with the lower layer. In between is a layer of negative perturbation. This vertical pattern can be intuitively explained using the perturbed static relation:

$$\Delta H' = (H'_2 - H'_1) = R \ln(P_1/P_2)\bar{T}'$$

where H, P, and T are geopotential height, pressure, and temperature; R is the universal gas constant; prime sign represents perturbation due to smoke; the subscripts 2 and 1 represent the top and bottom levels of a layer to be examined; over-bar represents layer average. For the lowest 2.5 km, $\bar{T}' < 0$, leading to $\Delta H' < 0$. This means that either $H'_2 < 0$ or $H'_1 > 0$, or both (that is, the geopotential height perturbation is either negative around 700 hPa or positive around 900 hPa or both). In contrast, for the layer between 2.5 and 5 km, $\bar{T}' > 0$, leading to $\Delta H' > 0$. This means that either $H'_2 > 0$ or $H'_1 < 0$, or both (that is, the perturbation is either positive around 500 hPa or negative around 700 hPa, or both).

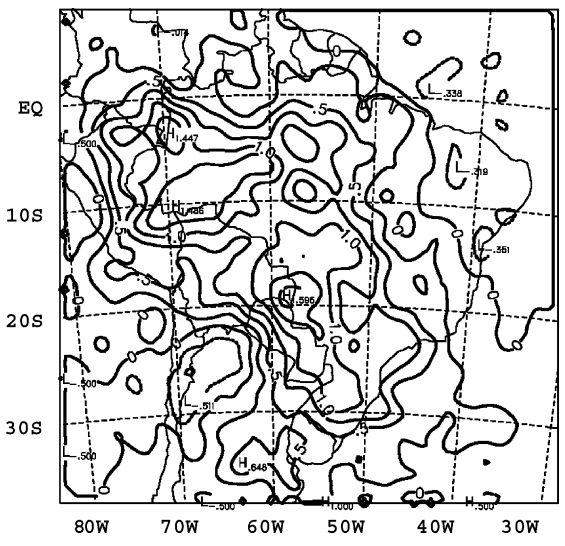

Fig. 10. Geographic pattern of perturbation in the 500 hPa geopotential height (m) due to smoke. The contour interval is 0.5 m.

The original vertical component of the atmospheric velocity averaged over the smoke region is negative above about 1.5 km (Fig. 8(h)), meaning that the atmosphere above PBL is dominated by subsidence due to the control of the Atlantic Ocean high. The largest descending speed is nearly −0.5 mm/s at the height of 4 km. Meanwhile, there is ascending motion in PBL. Smoke leads to a subsidence tendency in the lowest 4 km. The negative perturbation in geopotential height around 700 and the positive perturbation around

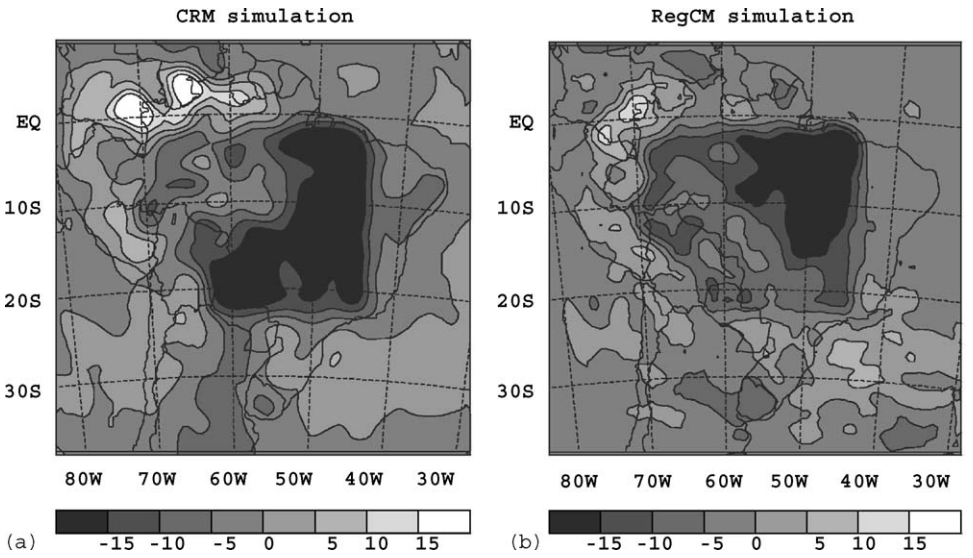

Fig. 11. Direct radiative forcing of smoke (W m^{-2}) with atmospheric feedback. Panel (a) is the difference in the net solar radiation flux at the top model level between the CRM smoke-feedback and control simulations, and panel (b) is the difference between the RegCM smoke and control simulations.

900 hPa imply a tendency of horizontal air mass convergence and divergence, respectively. So the downward motion is generated between the two elevations. This subsidence tendency is another contributor in addition to the reduced relative humidity to the reduction in clouds when smoke is present.

4.4. Feedback of atmospheric perturbation

In comparison with the DRF without atmospheric feedback (Fig. 5), the magnitude of the DRF with atmospheric feedback (Fig. 11(a)) is remarkably reduced over the smoke region, especially in the western portion. The average over the smoke region is -9.8 W m^{-2}, only about two thirds of that without atmospheric feedback. In the northwestern area outside the smoke region, radiative forcing with atmospheric feedback even turns to positive with a large magnitude of 15 W m^{-2}, resulting from the reduction in clouds due to smoke. More solar radiation is allowed to reach the surface in the less-cloud atmosphere.

The role of atmospheric feedback can also be analyzed by comparing the perturbation in the net solar radiation flux at the top model level simulated using RegCM (Fig. 11(b)), which includes the effect of atmospheric feedback on the smoke radiative forcing. The extent of large magnitude of negative perturbation in this figure is much smaller. The average over the smoke region is -9.8 W m^{-2} (Fig. 6), about the same as the DRF with atmospheric feedback simulated using CRM. The net long-wave radiation at the top model level is also changed due to the perturbations in air temperature and clouds due to smoke, but the magnitude is only about 0.6 W m^{-2}. Note that the land-surface conditions are specified in CRM but calculated in RegCM. Also CRM uses the RegCM outputs averaged over the integration period rather than those at each time step. These factors can also cause differences in the radiative forcing between the CRM and RegCM simulations.

4.5. Dependence on absorption

Herring and Hobbs (1994) found an upward movement of radiative-convective mixing layer generated within the Kuwait oil–fire plumes. This movement, however, is not found in the vertical motion perturbation due to smoke simulated with RegCM (Fig. 8(h)). When SSA is reduced to 0.82 for young smoke (the RegCM smoke simulation–strong absorption), however, ascending motion is generated above 2 km (Fig. 12) on top of a subsidence layer. This structure was obtained by an analytical model as well (Liu, 2003). In contrast, when SSA is increased to 0.94 for aged smoke (RegCM smoke simulation–weak absorption), the descending motion above the ground shown in Fig. 8(h) becomes more intense.

Absorption intensity also affects other atmospheric fields. In general, stronger (weaker) absorption leads to smaller (larger) magnitude of perturbations in air

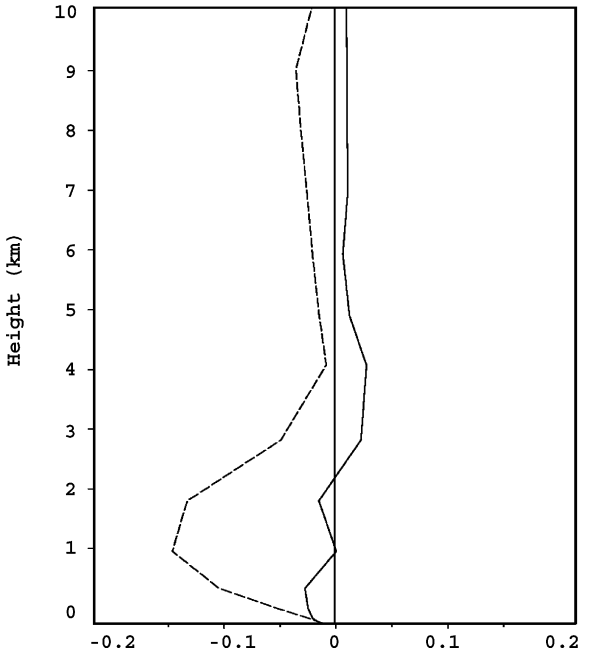

Fig. 12. Vertical profile of vertical velocity perturbation averaged over the smoke region (mm/s). The solid (dashed) line represents the difference between the smoke-strong (smoke-weak) absorption and control simulations.

temperature, geopotential height, humidity in the cloud layer, and cloud water path.

5. Discussion

The reduction in clouds due to smoke simulated with RegCM provides modeling evidence for a recent finding from satellite remote sensing. Koren et al. (2004) found dramatic changes in clouds due to smoke in Amazon based on the MODIS satellite measurements. Cloud fraction during the biomass-burning season was reduced from 38% in clean conditions to 0% for heavy smoke. The mechanism for the reduction of clouds in the Amazon due to smoke is an important issue for understanding the climatic effects on and feedback to the radiative forcing of smoke. A mechanism was proposed by Koren et al. (2004) to interpret their finding, which was a combination of a few dependent feedback processes, including stabilization of the atmosphere due to smoke absorption of solar radiation, reduction in evapotranspiration and the moisture input into the atmosphere, and decreased chance of super-saturation due to either increased capacity of the atmosphere in holding water vapor or enhanced competition for water vapor by increased particle number. The simulation with RegCM indicates that the reduction in relative humidity and subsidence tendency at the cloud layer are two major contributors.

The role of relative humidity was first noticed when examining the ''cloud burning'' mechanism proposed to connect soot to the cloud reduction over the Indian Ocean during INDOEX (Ackerman et al., 2000). The absorption of solar radiation by the soot increases air temperature and, therefore, reduces relative humidity. As a result, clouds are burned out in the drying atmosphere. For the cloud reduction in tropical South America obtained from the RegCM simulation, however, the major cause for the reduction in relative humidity is different: the reduced water vapor transport from the ground and PBL to the cloud layer due to the combined effects of the weaker turbulent activity and the subsidence tendency, is more important than perturbation in air temperature in tropical South America.

The cloud reduction due to smoke has some important implications for global and regional radiative balance and climate change. The simulated DRF without atmospheric feedback is $-16.5\ \mathrm{W\ m^{-2}}$, comparable to the value of $-15 \pm 5\ \mathrm{W\ m^{-2}}$ from an atmospheric radiative transfer model with a total optical depth of 0.75 for the 1995 Amazon smoke season (Ross et al., 1998). The magnitude of its global average is much smaller than that of an early estimate of $-1\ \mathrm{W\ m^{-2}}$ (Penner et al., 1992), suggesting a smaller role of tropical biomass burning in global radiation budget. If the feedback of cloud reduction is included, smoke DRF is changed to $-9.8\ \mathrm{W\ m^{-2}}$. This smaller magnitude, which is close to the measured values between -5 and $-12\ \mathrm{W\ m^{-2}}$ of clear-sky direct radiative forcing during dry seasons of 7 years at two Amazon locations heavily impacted by biomass burning (Procopio et al., 2004), indicates an even smaller role of the biomass burning in global radiation budget.

The cloud reduction due to biomass burning could be a factor for the monsoon process in the South America, which usually starts shortly after smoke seasons. The cloud reduction and the associated rainfall reduction will modify soil moisture, which has the capacity to retain anomalous signals in the land–atmosphere system at monthly and seasonal scales (Liu and Avissar, 1999). Thus, perturbations in the land–atmosphere system caused by biomass burning can last a few months beyond a smoke season and, therefore, affect the monsoon process. It is expected that soil moisture is reduced in response to the rainfall reduction during a smoke season, which then leads to reduction in rainfall during the coming monsoon season.

6. Conclusions

The numerical simulations with the NCAR regional climate model have been conducted to investigate the effects of smoke aerosols from biomass burning during the 1995 dry season in tropical South America on atmospheric radiation and regional climate. It is concluded that:

a. Smoke from biomass burning in the Amazon can significantly affect regional shortwave radiation budget. The magnitude of the impact, however, is substantially reduced because of atmospheric feedback, which is more significant in the western Amazon region.
b. Cloud water path is reduced in response to the radiative forcing of smoke, in agreement with the satellite measurements. The weaker water transfer from the ground and PBL to the cloud layer and subsidence tendency due to smoke are major contributors.
c. The intensity of smoke absorption can change the structure of the perturbation in atmospheric thermodynamics. Smoke with strong absorption generates a two-layer structure in the perturbed atmospheric fields, characterized by an ascending motion tendency of warming air on top of a descending motion tendency of cooling air.

Acknowledgements

The author wishes to thank two anonymous reviewers for their valuable comments and suggestions, which substantially improved this manuscript. This study was supported by the USDA Forest Service National Fire Plan through the Southern High-Resolution Modeling Consortium (SHRMC) and by the U.S. National Science Foundation (Award 0203761). The editorial support from Ken Forbus is appreciated.

References

Ackerman, A.S., Toon, O.B., Stevens, D.E., Heymsfield, A.J., Ramanathan, V., Welton, E.J., 2000. Reduction of tropical cloudiness by soot. Science 288, 1042–1047.

Andreae, M.O., Merlet, P., 2001. Emission of trace gases and aerosols from biomass burning. Global Biogeochem. Cycl. 5, 955–966.

Andreae, M.O., Rosenfeld, D., Artaxo, P., Costa, A.A., Frank, G.P., Longo, K.M., Silva-Dias, M.A.F., 2004. Smoking rain clouds over the Amazon. Science 303, 1337–1342.

Anthes, R.A., Hsie, E.-Y., Kuo, Y.-H., 1987. Description of the Penn State/NCAR Mesoscale Model Version 4(MM4), Technical Note, NCAR/TN-282 + STR, National Center for Atmospheric Research, Boulder, Colorado, 66 pp.

Charlson, R.J., Schwartz, S.E., Hales, J.M., Cess, R.D., Coakley Jr., J.A., Hansen, J.E., Hoffman, D.J., 1992. Climate forcing by anthropogenic sulfate aerosols. Science 255, 423–430.

Crutzen, P.J., Andreae, M.O., 1990. Biomass burning in the tropics: impact on atmospheric chemistry and biogeochemical cycles. Sciences 250, 1669–1678.

Davison, P.S., Roberts, D.L., Arnold, R.T., Colvile, R.N., 2004. Estimating the direct radiaitve forcing due to haze from the 1997 forest fires in Indonesia. J. Geophys. Res. 109, D10207 doi: 10.1029/2003JD004264.

Dickinson, R.E., Errico, R.M., Giorgi, F., Bates, G.T., 1989. A regional climate model for the western U.S. J. Clim. 15, 383–422.

Dickinson, R.E., Henderson-Sellers, A., Kennedy, P.J., 1993. Biosphere–Atmosphere Transfer Scheme (BATS) Version 1E as Coupled to the NCAR Community Climate Model, NCAR Tech. Note/TN-387, National Center for Atmospheric Research, Boulder, CO, 72 pp.

Eck, T.F., Holben, B.N., Slutsker, I., Setzer, A., 1998. Measurements of irradiarance attenuation and estimation of aerosol single scattering albedo for biomass burning aerosols in Amazonia. J. Geophys. Res. 103, 31865–31878.

Giorgi, F., Bates, G.T., 1989. The climatological skill of a regional model over complex terrain. Mon. Wea. Rev. 117, 2325–2347.

Giorgi, F., Huang, Y., Nishizawa, K., Fu, C., 1999. Seasonal cycle simulation over eastern Asia and its sensitivity to radiative transfer and surface processes. J. Geophys. Res. 104, 6403–6424.

Giorgi, F., Bi, X., Qian, Y., 2002. Direct radiative forcing and regional climatic effects of anthropogenic aerosols over East Asia: a regional coupled climate-chemistry/aerosol model study. J. Geophys. Res. 107 (D20), 4439 doi: 10.1029/2001JD001066.

Grell, A.G., 1993. Prognostic evaluation of assumptions used by cumulus parameterisations. Mon. Wea. Rev. 121, 764–787.

Grell, A.G., Dudhia, J., Stauffer, D.R., 1994. A Description of the Fifth-Generation Penn State/NCAR mesoscale Model (MM5), NCAR Tech. Note, 398, 122 pp.

Hansell, R.A., Tsay, S.-C., Ji, Q., Liou, K.-N., Ou, S.-C., 2003. Surface aerosol radiative forcing derived from collected ground-based radiometric observations during PRIDE, SAFARI, and ACE-Asia. Appl. Optics 42, 5533–5544.

Hansen, J., Sato, M., Ruedy, R., 1997. Radiative forcing and climate response. J. Geophys. Res. 102, 6831–6864.

Hao, W.M., Liu, M.-H., Crutzen, P.J., 1990. Estimates of annual and regional releases of CO2 and other trace gases to the atmosphere from fires in the tropics, based on the FAO statistics for the period 1975–1980. In: Goldammer, J.G. (Ed.), Fire in the Tropical Biota (Ecological Studies 94). Springer-Verlag, pp. 440–462.

Herring, J.A., Hobbs, P.V., 1994. Radiatively driven dynamics of the plume from 1991 Kuwait oil fires. J. Geophys. Res. 99, 18809–18826.

Hobbs, P.V., Reid, J.S., Kotchenruther, R.A., Ferek, R.J., Weiss, R., 1997. Direct radiative forcing by smoke from biomass burning. Science 275, 1176–1178.

Holben, B.N., Tanre, D., Smirnov, A., Eck, T.F., Slutsker, I., Abuhassan, N., Newcomb, W.W., Schafer, J.S., Chatenet, B., Lavenu, F., Kaufman, Y.J., Vande Castle, J., Setzer, A., Markham, B., Clark, D., Frouin, R., Halthore, R., Karneli, A., O'Neill, N.T., Pietras, C., Pinker, R.T., Voss, K., Zibordi, G., 2001. An emerging ground-based aerosol climatology: aerosols optical depth from AERONET. J. Geophys. Res. 106, 12067–12097.

Kaufman, Y.J., Tanre, D., 1994. Variations in cloud supersaturation and the aerosol indirect effect on climate. Nature 369, 45–48.

Kaufman, Y.J., Hobbs, P.V., Kirchhoff, V.W.J.H., Artaxo, P., Remer, L.A., Holben, B.N., King, M.D., Ward, D.E., Prins, E.M., Longo, K.M., Mattos, L.F., Nobre, C.A., Spinhirne, J.D., Ji, Q., Thompson, A.M., Gleason, J.F., Christopher, S.A., Tsay, S.-C., 1998. Smoke, clouds, and radiation-Brazil (SCAR-B) experiment. J. Geophys. Res. 103, 31783–31808.

Kiehl, J.T., Briegleb, B.P., 1993. The relative role of sulfate aerosols and greenhouse gases in climate forcing. Science 260, 311–314.

Kiehl, J.T., Schneider, T.L., Rasch, P.J., Barth, M.C., 2000. Radiative forcing due to sulfate aerosols from simulations with the National Center for Atmospheric Research Community Model, Version 3. J. Geophys. Res. 105, 1441–1457.

Kobayashi, H., Matsunaga, T., Hoyano, A., Aoki, M., Komori, D., Boonyawat, S., 2004. Satellite estimation of photosynthetically active radiation in Southeast Asia: impacts of smoke and cloud cover. J. Geophys. Res. 109, D04102 doi: 10.1029/2003JD003807.

Koren, I., Kaufman, Y.J., Remer, L.A., Martins, J.V., 2004. Measurement of the effects of Amazon smoke on inhibition of cloud formation. Science 303, 1342–1345.

Liu, Y.-Q., Avissar, R., Giorgi, F., 1996. A simulation with the regional climate model (RegCM2) of extremely anomalous precipitation during the 1991 East-Asian Flood: an evaluation study. J. Geophys. Res. 101, 26199–26215.

Liu, Y.-Q., Avissar, R., 1999. A study of persistence in the land–atmosphere system with a fourth-order analytical model. J. Clim. 12, 2154–2168.

Liu, Y.-Q., Liu, S.-C., Dickinson, R.E., 2000. Regional response of atmospheric circulation and surface energy and water balance to observed distribution of aerosol loading over the United States. In: Proceedings of the Seventh International Conference on Atmospheric Sciences and Applications to Air Quality (Abstracts), Taipei, Taiwan, October 2000, p. 178.

Liu, Y.-Q., 2003. Atmospheric response and feedback to smoke radiative forcing from wildland fires. In: Proceedings of the Second International Wildland Fire Ecology and Fire Management Congress, Amer. Meteor. Soc. Nov. 16–20, 2003, Orlando, FL, USA.

Liu, Y.-Q., 2004. Variability of wildland fire emissions across the continuous United States. Atmos. Environ. 38, 3489–3499.

Menon, S., Hansen, J.E., Nazarenko, L., Luo, Y., 2002. Climate effects of black carbon aerosols in China and India. Science 297, 2250–2253.

Moraes, E.C., Franchito, S.H., Rao, V.B., 2004. Effects of biomass burning in Amazonia on climate: a numerical experiment with a statistical–dynamical model. J. Geophys. Res. 109, D05109 doi: 10.1029/2003JD003800.

Murray, F.W., 1967. On the computation of saturation vapor pressure. J. Appl. Meteorol. 6, 203–204.

Penner, J.E., Dickinson, R.E., O'Neill, C.S., 1992. Effects of aerosol from biomass burning on the global radiation budget. Science 256, 1432–1434.

Procopio, A.S., Artaxo, P., Kaufman, Y.J., Remer, L.A., Schafer, J.S., Holben, B.N., 2004. Multiyear analysis of Amazonian biomass burning smoke radiaitve forcing of climate. J. Geophys. Res. 31, L03108 doi: 10.1029/2003GL018646.

Qian, Y., Giorgi, F., 1999. Interactive coupling of regional climate and sulfate aerosol models over eastern Asia. J. Geophys. Res. 104, 6477–6500.

Radke, L.F., Hegg, D.A., Hobbs, P.V., Nance, J.D., Lyons, J.H., Laursen, K.K., Weiss, R.E., Riggan, P.J., Ward, D.E., 1991. Particulate and trace gas emissions from large biomass fires in North America. In: Levine, J.S. (Ed.), Global Biomass Burning: Atmospheric, Climatic, and Biospheric Implications. The MIT Press, pp. 209–224.

Ross, J.L., Hobbs, P.V., Holben, B., 1998. Radiative characteristics of regional hazes dominated by smoke from biomass burning in Brazil: closure tests and direct radiative forcing. J. Geophys. Res. 103, 31925–31941.

Seiler, W., Crutzen, P.J., 1980. Estimates of grassland net fluxes of carbon between the biosphere and the atmosphere from biomass burning. Clim. Change 2, 207–247.

Shea, D.J., Trenberth, K.E., Reynolds, R.W., 1992. A global monthly sea surface temperature climatology. J. Clim. 5, 987–1001.

Sinha, P., Jaege, L., Hobbs, P.V., Liang Q., 2004. Transport of biomass burning emissions from Southern Africa. J. Geophys. Res. 109, D20204 doi: 10.1029/2004JD005044.

Swap, R.J., Annegarn, H.J., Suttles, J.T., King, M.D., Platnick, S., Privette, J.L., Scholes, R.J., 2003. Africa burning: a thematic analysis of the Southern African Regional Science Initiative (SAFARI 2000). J. Geophys. Res. 108 (D13), 8465 doi: 10.1029/2003JD003747.

Trosnikov, I.V., Nobre, C.A., 1998. Estimation of aerosol transport from biomass burning aeros during the SCAR-B experiment. J. Geophys. Res. 103, 32129–32137.

Twomey, S., Piepgrass, M., Wolfe, T.L., 1984. An assessment of the impact of pollution on global cloud albedo. Tellus 36B, 356–366.

Ward, D.E., Setzer, A.W., Kaufman, Y.J., Rasmussen, R.A., 1991. Characteristics of smoke emissions from biomass fires of the Amazon region-BASE-A experiment. In: Levine, J.S. (Ed.), Global Biomass Burning: Atmospheric, Climatic, and Biospheric Implications. The MIT Press, pp. 394–402.